Applied Catalysis B: Environmental 123–124 (2012) 316–323

Contents lists available at SciVerse ScienceDirect

Applied Catalysis B: Environmental

journal homepage: www.elsevier.com/locate/apcatb

# Mesoporous tantalum phosphate as acidic catalyst for the methanolysis of sunflower oil

I. Jiménez-Morales, J. Santamaría-González, P. Maireles-Torres, A. Jiménez-López*

*Departamento de Química Inorgánica, Cristalografía y Mineralogía (Unidad Asociada al ICP-CSIC), Facultad de Ciencias, Universidad de Málaga, Campus de Teatinos, 29071 Málaga, Spain*

ARTICLE INFO

*Article history:*
Received 20 February 2012
Received in revised form 12 April 2012
Accepted 19 April 2012
Available online 25 April 2012

*Keywords:*
Mesoporous tantalum phosphate
Transesterification
Sunflower oil
Acid catalysts

ABSTRACT

Mesoporous tantalum phosphate was prepared from tantalum tartrate complex and ammonium dihydrogenphosphate, by using hexadecyltrimethylammonium bromide as surfactant, and ulterior calcination at 550 °C. It exhibits a high specific surface area (256 $m^2 g^{-1}$) and strong acidity (1480 μmol $NH_3 g^{-1}$), and it can be successfully used as solid catalyst in the transesterification of sunflower oil with methanol. With only 5 wt.% of this catalyst in relation to the oil, a 89 wt.% of biodiesel formation was attained at 200 °C and after only 2 h of reaction. The catalyst is very stable and no leaching of tantalum or phosphorus species to the liquid medium was found. Moreover, this acid solid catalyst is able to simultaneously catalyse the esterification of free fatty acids (FFAs) and the transesterification of triglycerides, even in the presence of 9% of FFAs. Its catalytic performance is well maintained after three catalytic cycles, without any treatment and even in the presence of 5 wt.% of water. The use of a co-solvent do not enhanced the biodiesel formation.

© 2012 Elsevier B.V. All rights reserved.

## 1. Introduction

Biodiesel is a renewable fuel consisting of monoalkyl esters of fatty acids with methanol, produced from biomass feedstocks such as vegetable oils or animal fats. However, the overall production cost are still very high compared to petroleum-based diesel fuel, owing to both the high price of raw materials and processing [1]. The first cost can be reduced by using feedstock like waste cooking oil, although this contains undesirable compounds such as free fatty acids (FFAs) and water [2,3].

Homogeneous base catalysis is the more developed industrial process, but it is inappropriate when the feedstock is cooking oil because the presence of moisture and FFAs induce consuming of catalyst by saponification and formation of emulsions. For this type of feedstock, acid catalysts are preferable because they can simultaneously carry out esterification of FFAs and transesterification of triglycerides under appropriate conditions. However, the reaction rate with homogeneous acid catalysis is slow, requires high temperatures, high alcohol/oil molar ratios, neutralisation and separation steps.

Solid acid catalysts, which are easily recovered from the reaction system, are an emerging group of catalysts that, in some cases, exhibit reactivity for biodiesel production, thus combining green chemistry features and economic viability [4,5]. Several authors have reviewed the application of different heterogeneous acid catalysts to the biodiesel preparation such as Lotero et al. [6], Santacesaria and co-workers [7], Melero et al. [8] and Mbaraka and Shanks [9]. Among the most studied acidic solids are resins [10], tungstated zirconia [11–13], sulphated zirconia [14,15], zirconium sulphate [16,17], heteropolyacids [18–20], etc.

Recently, several compounds based on elements of the 5th group of the Periodic Table have been employed as catalysts in the biodiesel production. Thus, α-$VOPO_4 \cdot 2\,H_2O$ activated at 500 °C was tested in the catalytic transesterification reaction of soybean oil with methanol at 150–180 °C during 1 h [21]. The dehydration of this phase has a positive effect on the activity attaining yields of biodiesel close to 80% at these moderate temperatures. However, a low deactivation has been experimentally observed under the reaction conditions owing to the partial reduction of V(V) to V(III) by methanol, although catalysts can be easily regenerated by calcination in air.

On the other hand, the so-called "niobic acid" ($Nb_2O_5 \cdot nH_2O$) and niobium phosphates are solids with strong acidic properties due to the presence of water molecules, thus can be used as solid acid catalysts [22,23]. In this sense, niobic acid calcined at temperatures as low as 300 °C possesses an acid strength equivalent to 70% of sulfuric acid. Moreover, its acid treatment with sulfuric or phosphoric acid causes an enhancement of its acid strength up to 90% of sulfuric acid. These promoted solids have been assayed as catalysts in the esterification of oleic acid with methanol at 70 °C. Although the yield of this reaction is only

* Corresponding author. Tel.: +34 952131876; fax: +34 952131870.
*E-mail address:* ajimenezl@uma.es (A. Jiménez-López).

0926-3373/$ – see front matter © 2012 Elsevier B.V. All rights reserved.
http://dx.doi.org/10.1016/j.apcatb.2012.04.023

40%, the activity is well maintained during 5 cycles of reaction [24].

$Ta_2O_5{\cdot}nH_2O$ has been also used as support of acidic species such as polyoxometalates, due to its intrinsic acid properties which are enhanced by incorporation of these species via Ta—O—W bonds. Thus, mesoporous $H_3PW_{12}O_{40}/Ta_2O_5$ solids, prepared by a one-step sol–gel-hydrothermal method in the presence of triblock copolymer surfactants, are active in both the esterification of lauric acid and the transesterification of soybean oil with methanol. These catalysts are stable against leaching of the Keggin unit into the polar reaction media [25,26], they can be recovered, reactivated and reused several times. Moreover, the catalytic performance can be still improved by the incorporation of hydrophobic alkyl groups terminally bonded on $Ta_2O_5$ via Ta—O—Si—R. The resulting organo-inorganic hybrid catalysts exhibited much higher catalytic reactivity for transesterification reaction compared with polyoxometalate/$Ta_2O_5$ one. This excellent catalytic performance is due to its enhanced acid strength and its hydrophobic character compared with the not functionalised counterparts [27,28].

Recently, we reported the synthesis and characterisation of new catalysts based on $Nb_2O_5$ or $Ta_2O_5$ supported on MCM-41 and SBA-15, respectively, and their application to the transesterification of sunflower oil with methanol at 200 °C with good yields of biodiesel [29,30]. These catalysts were reutilised several times and are stable since no leaching of the active phases were found.

The goal of the present research is the application of a mesoporous tantalum phosphate molecular sieve [31] for the preparation of biodiesel from sunflower oil with methanol, under heterogeneous acid–catalysis reaction. The use of ordered mesoporous catalysts presents significant advantages with respect to conventional ones, due to its high specific surface area and large pore size which lead to a better diffusion of reactants [32]. The influence of the thermal treatment on the acidic properties of this catalyst, as well as the study of several experimental parameters such as reaction temperature, reaction time, percentage of catalyst, reutilisation and the presence of free fatty acids, water and co-solvent have been evaluated to optimise the experimental conditions for biodiesel production.

## 2. Experimental

### 2.1. Synthesis of mesoporous tantalum phosphate

The mesoporous tantalum phosphate was prepared by using tantalum penta-ethoxide as source of tantalum. This was transformed into the corresponding tartrate complex by reaction with tartaric acid in absolute ethanol, employing a tartaric acid/tantalum molar ratio = 3. Then, the solvent was evaporated till a minimum volume before precipitation, and water was added. The mesoporous tantalum phosphate was prepared according to the method reported by Sarkar and Pramanik [31]: a solution of 0.012 mol of tantalum tartrate in 38 mL of water was treated with 4 g of diammonium hydrogen phosphate, previously dissolved in 14 mL of distilled water, under constant stirring until a homogeneous clear solution was obtained. Then, 1.4 g of hexadecyltrimethylammonium bromide dissolved in 15 mL of distilled water was added with vigorous stirring during 30 min. The white precipitate was annealed in a Teflon autoclave at 130 °C during 24 h. The resulting solid was then filtered and washed with distilled water and alcohol, and dried at 60 °C. The surfactant employed to form the mesostructured organo-inorganic hybrid precursor was eliminated by calcination at 550 °C during 6 h. The mesoporous tantalum phosphate obtained was kept in equilibrium with an atmosphere of 55% humidity.

### 2.2. Characterisation techniques

X-ray diffraction (XRD) patterns of catalysts were collected on a PAN analytical X'Pert Pro automated diffractometer. Powder patterns were recorded in Bragg–Brentano reflection configuration by using a Ge (1 1 1) primary monochromator (Cu $K\alpha_1$) and the X'Celerator detector with a step size of 0.017° ($2\theta$), The XRD patterns were obtained at low angles, between 0.5° and 10° in $2\theta$, with an equivalent counting time of 204.8 s/° and at high angles, between 10° and 70° in $2\theta$, with 29.6 s/°.

The thermodiffractometric study of mesoporous tantalum phosphate was carried out using an Anton Paar HTK1200 Camera under static air. Flux of gases was not employed to avoid sample dehydration prior to the diffraction experiment. Data were collected at different temperature intervals, ranging between 30 and 1000 °C with a heating rate of 10 °C $min^{-1}$ and maintaining 15 min at each desired temperature to ensure thermal stabilisation. The data acquisition range was 8–70° ($2\theta$) with a step size of 0.017°.

Thermogravimetric (TG) and differential thermal analysis (TDA) of the mesoporous tantalum phosphate precursor were performed in air from r.t. until 900 °C on a SDT Q600 apparatus from TA Instruments; calcined alumina as a reference and a heating rate of 10 °C $min^{-1}$ were employed.

The textural parameters were evaluated from nitrogen adsorption–desorption isotherms at −196 °C, as determined by an automatic ASAP 2020 system from Micromeritics. The accumulated pore volumes were determined by BJH method. The total acidity of catalysts were measured by temperature-programmed desorption of ammonia ($NH_3$-TPD). Catalysts (80 mg) were pre-treated at atmospheric pressure by flowing helium (35 ml $min^{-1}$) from room temperature to 550 °C, with a heating rate of 10 °C $min^{-1}$, and maintaining the sample at 550 °C for 1 h. Then, catalysts were cooled until 100 °C under a helium flow and ammonia was adsorbed at this temperature. The desorption of adsorbed ammonia was carried out from room temperature to 550 °C, with a heating rate of 10 °C $min^{-1}$ and maintaining the sample at 550 °C for 15 min. The evolved ammonia was analysed by on-line gas chromatograph (Shimadzu GC-14A) provided with a TCD.

FTIR spectra of catalysts were recorded on a Shimadzu Fourier Transformation Instrument (FTIR-8300) using self supported wafers of the samples. The obtained discs were placed in a greaseless stopcocks vacuum cell with $CaF_2$ windows. The samples were evacuated during 3 h at different temperatures: r.t., 250 and 375 °C. For the study of the adsorption of pyridine coupled to FTIR spectroscopy, self-supported wafers of samples with a weight/surface ratio of about 15 mg $cm^{-2}$ were placed in a greaseless stopcocks vacuum cell provided with $CaF_2$ windows. The samples were evacuated at r.t., 250 °C and 375 °C and $10^{-2}$ Pa during 6 h, exposed to pyridine vapours at room temperature for 15 min and then outgassed at different temperatures.

Raman spectra were obtained with a Raman Senterra (Bruker) micro-spectrometer equipped with a thermoelectrically cooled CCD detector. Excitation radiation at 1064 nm was used as supplied from a Praseodimium laser. Raman spectra were performed from powder samples without any previous treatment.

X-ray photoelectron spectra were collected using a Physical Electronics PHI 5700 spectrometer with non-monochromatic Al Kα radiation (300 W, 15 kV, 1486.6 eV) with a multi-channel detector. Spectra of samples were recorded in the constant pass energy mode at 29.35 eV, using a 720 μm diameter analysis area. Charge referencing was measured against adventitious carbon (C 1s at 284.8 eV). A PHI ACCESS ESCA-V6.0 F software package was used for acquisition and data analysis. A Shirley-type background was subtracted from the signals. All recorded spectra were always fitted using Gaussian–Lorentzian curves to more accurately

determine the binding energy of the different element core levels.

### 2.3. Catalytic test

The methanolysis of edible sunflower oil was performed at 200 °C by using a Parr high pressure reactor with 100 mL capacity and a stirring rate of 600 rpm. Before reaction, catalysts were kept in equilibrium with an atmosphere of 55% humidity or activated in air at 375 °C during 1 h. In a typical experiment, 10 g of oil was incorporated to the reactor together with the methanol and 0.5 g of catalyst. The methanol/oil molar ratio was 12. After 4 h of reaction, the system was cooled and an aliquot (2 mL) was taken and treated with 1 mL of distilled water and shaking for few minutes. Later, 1 mL of dichloromethane was added, and this mixture was again agitated and set aside to develop two phases: the non-polar phase containing dichloromethane, mono-, di- and triglycerides and methyl esters of fatty acids (FAME) (and traces of methanol and glycerol) and the polar phase containing water, glycerol and methanol (and traces of esters). The dichloromethane was then removed from the organic phase by evaporation at 90 °C. The resulting solution was analysed by high performance liquid chromatography (HPLC) using a JASCO liquid chromatograph equipped with quaternary gradient pump (PU-2089), multiwavelength detector (MD-2015), autosampler (AS-2055), column oven (co-2065) using a PHENOMENEX LUNA C18 reversed-phase column (250 mm × 4.6 mm, 5 μm). The solvents were filtered through a 0.45 μm filter prior use and degassed with helium. A linear gradient from 100% methanol to 50% methanol + 50% 2-propanol/hexane (5:4, v/v) in 35 min was employed. Injection volumes of 15 μL and a flow of rate of 1 mL $min^{-1}$ were used. The column temperature was held constant at 40 °C. All samples were dissolved in 2-propanol–hexane (5:4, v/v). The weight content in FAME determined by HPLC was considered to represent the FAME yield (in wt.%) of the catalytic process, assuming that, during the neutralisation and the washing process of the ester phase, only traces of esters were transferred to the polar phase and that only the extraction of methanol and glycerol take place.

The degree of leaching of tantalum phosphate was measured by using an ICP-MS ELAN DRCe equipment (PerkinElmer) and employing the following parameters: RF power = 1100 W, argon plasma gas flow = 15.0 L $min^{-1}$, auxiliary gas flow = 0.9 L $min^{-1}$ and sample uptake rate = 0.9 mL $min^{-1}$.

## 3. Results and discussion

### 3.1. Catalyst characterisation

The DTA curve of the mesoporous tantalum phosphate, obtained after calcination at 550 °C to eliminated the surfactant and kept in equilibrium with an atmosphere of 55% humidity, presents two endothermal effects centred at 85 °C and 200 °C, associated to the loss of hydration and coordinated water molecules, respectively (Fig. 1). The TG curve indicates a continuous weight loss from room temperature till 600 °C. The weight loss associated to hydration water is 4.7 wt.%, whereas that corresponding to coordinated water, observed between 150 °C and 600 °C, represents 1.82 wt.%. This last data clearly indicates that the coordinated water is strongly retained since it requires high temperatures to be eliminated. That leads to a chemical composition for the dry compound of $TaOPO_4 \cdot 0.30\ H_2O$, which reveals that not all the tantalum atoms are able to coordinate a water molecule, possibly due to the fact that they are interacting with other Ta=O groups forming the walls of the mesoporous structure, in similar way that occurs in the tetragonal anhydrous $TaOPO_4$ [33]. When coordinated water is eliminated,

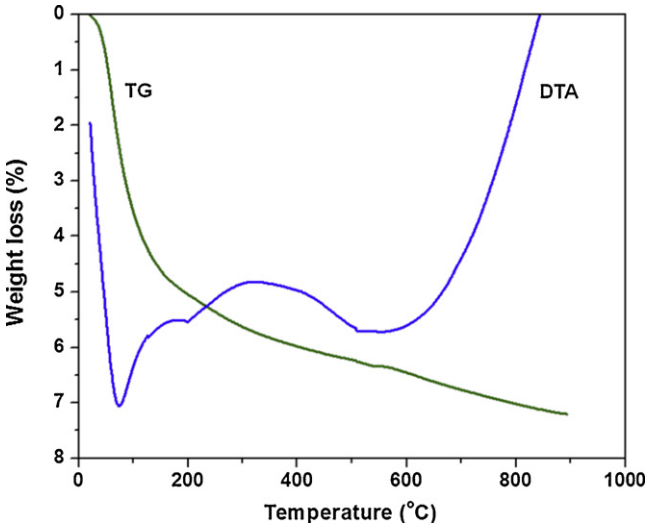


**Fig. 1.** TG and DTA curves of mesoporous tantalum phosphate.

the formation of a more disordered structure takes place, appearing an amorphous $TaOPO_4$ which is responsible of the broad exothermal effect observed in the DTA curve at higher temperatures.

X ray diffraction patterns in the low angle region of the mesoporous tantalum phosphate exhibits an intense peak at $2\theta = 1.3°$, typical of a mesoporous structure (Fig. 2). Thus, the corresponding inter-planar spacing $d_{100}$ of this hexagonal arrangement is 6.69 nm, which is higher than that obtained when tetradecyltrimethylammonium is used as template [31], owing to the longer alkyl chain of the surfactant employed in our synthesis, hexadecyltrimethylammonium bromide. In the high angle region, typical broad bands of amorphous solids are observed at 22° and 35°. A thermodiffractometry study of the mesoporous tantalum phosphate was also run from 500 °C till 1000 °C (Fig. 3). In all cases, the XRD patterns did not show new peaks. The tetragonal $TaOPO_4$ solid, which is formed after heating of the analogous lamellar niobium phosphate, does not appear [34], because its synthesis requires high pressures [33]. The characteristic diffraction peaks of tantalum pyrophosphate, observed when hydrous tantalum phosphate is calcined, were not detected either [35,36], indicating the high thermal stability of the mesoporous structure. In fact, after heating at 750 °C, the low angle diffraction peak is still observed, even at lower values as $2\theta = 1.26°$ (Fig. 2). However, when the sample is heated at 900 °C,

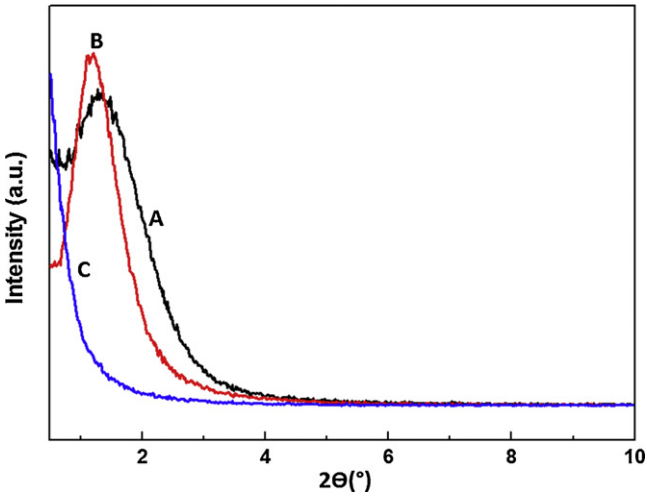


**Fig. 2.** XRD patterns at low angles of mesoporous tantalum phosphate activated at different temperatures: (A) r.t., (B) 750 °C and (C) 900 °C.

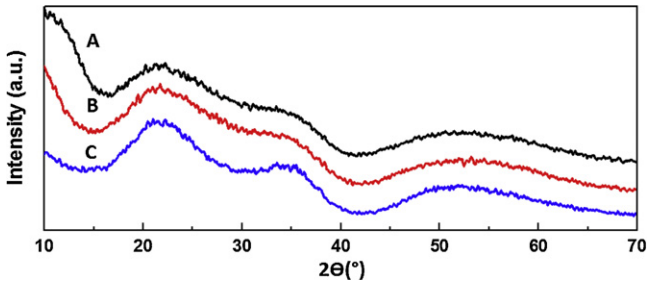


**Fig. 3.** XRD patterns at high angles of mesoporous tantalum phosphate activated at different temperatures: (A) r.t., (B) 750 °C and (C) 900 °C.

the mesoporous structure is collapsed since the peak at low angles disappeared, and possibly an amorphous $TaOPO_4$ is formed.

The chemical composition of the mesoporous tantalum phosphate was also determined by XPS analysis. The surface atomic percentages obtained are the following: O = 72.28%, P = 13.58 and Ta = 14.12%, which leads to the formula: $TaOPO_4 \cdot 0.32\ H_2O$, in very good agreement with the composition found from TG analysis. On the other hand, Fig. 4 depicts the XPS spectrum of tantalum in the core level region of Ta 4f where two peaks corresponding to Ta $4f_{7/2}$ and Ta $4f_{5/2}$ are observed at 26.3 and 28.2 eV, respectively [37,38]. The binding energies separation close to 1.9 eV and the area ratio of 1.36 confirm that Ta is fully oxidised as Ta(V). The O 1s signal appears as a large and asymmetrical peak centred at 531.6 eV which can be deconvoluted in two components at 531.1 eV and 532.5 eV (Fig. 4), which indicates two different oxide environments: oxygen bonded to phosphorous (531.1 eV) [39] and bonded to tantalum (532.5 eV), respectively. The areas ratio corresponding to both types

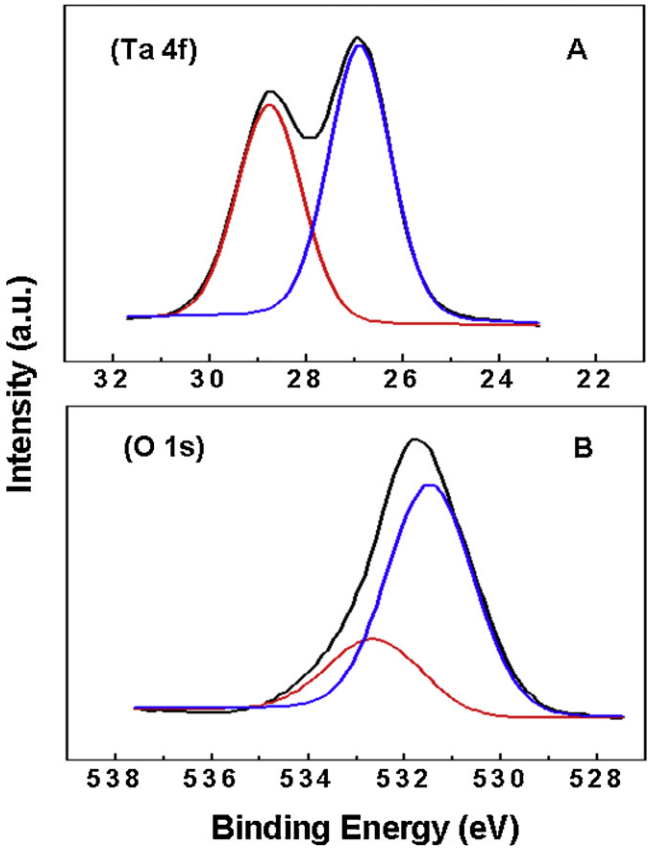


**Fig. 4.** (A) Ta 4f core level spectrum and (B) O 1s core level spectrum of mesoporous tantalum phosphate.

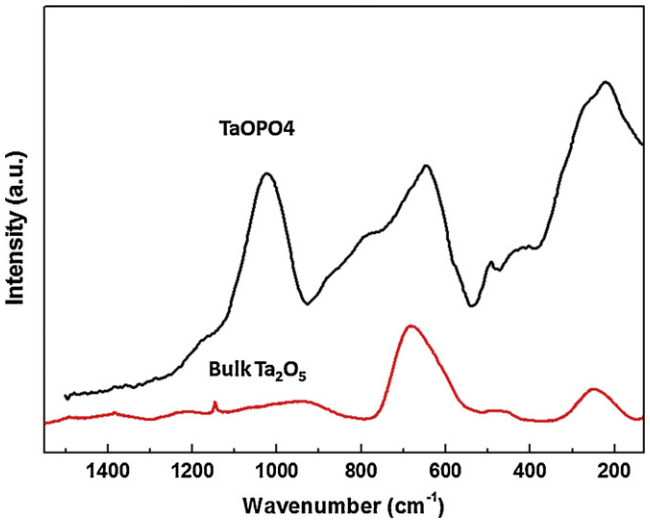


**Fig. 5.** Raman spectra of mesoporous tantalum phosphate and bulk $Ta_2O_5$.

of oxygen is 3.03 very close to that corresponding to the chemical composition above formulated.

The mesoporous tantalum phosphate was also characterised using laser Raman spectroscopy. The Raman spectrum of this solid together with that of a bulk tantalum pentaoxide, obtained by acid hydrolysis of the corresponding tantalum penta-ethoxide and calcination at 575 °C during 6 h, is shown in Fig. 5. The spectrum of bulk $Ta_2O_5$ in the range 200–1200 $cm^{-1}$ presents a major characteristic Raman band at 660 $cm^{-1}$ due to Ta—O vibrations. The shoulder at about 980 $cm^{-1}$ corresponds to the symmetric stretching mode of the terminal Ta=O bonds [40]. These features are also observable in the mesoporous tantalum phosphate, although the phosphate groups also exhibit stretching vibration bands in the same region, 984–1013 $cm^{-1}$ [41].

FTIR analysis was also carried out to investigate the chemical nature of mesoporous tantalum phosphate, which was kept in equilibrium with an atmosphere of 55% humidity (Fig. 6). The broad and intense band centred at 1041 $cm^{-1}$ contains both the $\nu_3$ stretching band of tetrahedral phosphate groups and the stretching vibrations of Ta=O groups. The bands at 643 $cm^{-1}$ and 517 $cm^{-1}$ correspond to the stretching vibrations of Ta—O bonds [42]. The vibration band corresponding to the deformation of water molecules appears at 1638 $cm^{-1}$, which is associated to the broad

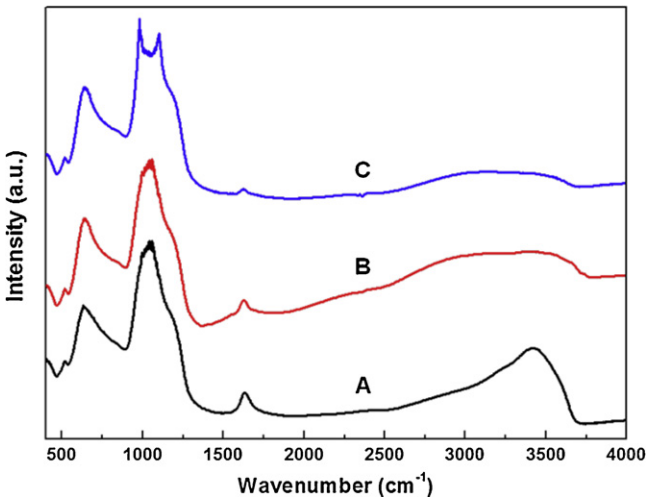


**Fig. 6.** FTIR spectra of mesoporous tantalum phosphate evacuated at different temperatures: (A) r.t., (B) 250 °C and (C) 375 °C.

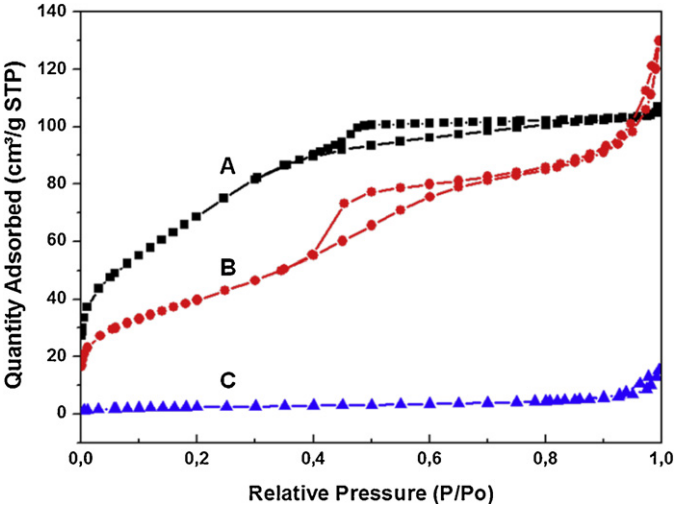


**Fig. 7.** Adsorption isotherms of $N_2$ at −196 °C of mesoporous tantalum phosphate, activated at: (A) r.t., (B) 750 °C and (C) 900 °C.

band centred at 3422 $cm^{-1}$ due to the stretching of OH groups. After heating at 375 °C, the intensity of vibration bands associated to water molecules decreased, but the persistence of the band at 1638 $cm^{-1}$ reveals that some coordinated water is still retained, as was inferred from the TG study. At the same time, the band centred at 1041 $cm^{-1}$ splits in two absorption components at 1099 and 981 $cm^{-1}$, which can be assigned to the $\nu_3$ of phosphate groups [43] and the Ta=O stretching vibration modes, respectively [44]. The shoulder at 1250 $cm^{-1}$ could be assigned to δ P—OH of uncoordinated phosphate groups.

The textural parameters of mesoporous tantalum phosphate, after thermal treatment at different temperatures, deduced from the $N_2$ sorption at −196 °C, are summarised in Table 1. The $N_2$ adsorption–desorption isotherms of the mesoporous tantalum phosphate, before and after activation at 750 °C, are similar and belong to the type IV in the IUPAC classification, typical of mesoporous solids (Fig. 7). Although the amount of adsorbed nitrogen at low relative pressures decreased when the temperature of activation was 750 °C, at high relative pressure values, the amount of nitrogen adsorbed is higher, possibly due to the condensation of nitrogen molecules in pores and voids generated between agglomerates of particles formed after this thermal treatment. Thus, the BET surface area decreases with the increment of the calcination temperature, possibly due to the reorganisation and shrinkage of the mesoporous structure. In fact, the wall thickness of the mesoporous structure decreases when the temperature of treatment is raised (Table 1). At 900 °C, the mesoporous structure collapses, as was deduced from XRD analysis in the low-angle region, and the $N_2$ adsorption–desorption isotherm is typical of a non-porous solid and consequently the surface area is very low, only 8.3 $m^2\,g^{-1}$.

The acidity of the catalysts was measured by $NH_3$-TPD and the results are gathered in Table 1. The total acidity of the mesoporous tantalum phosphate is very high, attaining 1480 μmol $NH_3\,g^{-1}$. Taking into account that, previous to the adsorption of ammonia, samples were activated at 550 °C during 1 h, the loss of a majority of coordinated water molecules takes place; therefore, the amount of desorbed ammonia could correspond to the number of tantalum atoms able to coordinate an ammonia molecule. The total acidity value leads to the chemical composition $TaOPO_4$ 0.43 $NH_3$. This value is higher than that found for the coordinated water (0.30 mol/mol of phosphate), so that it could confirm the presence of some uncoordinated P—OH groups with acidic properties. After activation at 750 °C, the total acidity is reduced up to 989 μmol $NH_3\,g^{-1}$, as expected by considering a partial condensation of Ta=O groups with adjacent Ta atoms. Lastly, when the solid is treated at 900 °C and the formation of a collapsed structure occurs the acidity is very low, 371 μmol $NH_3\,g^{-1}$. At this temperature, the formation of an amorphous $TaOPO_4$ structure favours the full coordination of all the tantalum atoms, thus lowering the capacity to adsorb ammonia molecules.

The concentration of both Brönsted and Lewis acid sites has been determined by using adsorption of pyridine coupled to FTIR spectroscopy. As it is well known, the vibration band at 1550 $cm^{-1}$ is assigned to pyridinium ions formed on Brönsted acid sites, whereas that at 1450 $cm^{-1}$ corresponds to the pyridine coordinated to Lewis acid centres. The concentrations of both types of acid sites were estimated for the integrated absorption of both bands and using the extinction coefficients obtained by Dakta et al. [45], $E_B = 0.73\ cm\ mmol^{-1}$ and $E_L = 1.11\ cm\ mmol^{-1}$, for Brönsted and Lewis sites, respectively. The data compiled in Table 2 reveal that the mesoporous tantalum phosphate activated at different temperatures possesses both types of acid centres, being the concentration of Brönsted acid sites very high, even when the sample was evacuated at 375 °C before pyridine adsorption. On the one hand, this fact confirms that coordinated water is retained until high temperatures, as was observed in the FTIR spectrum of mesoporous tantalum phosphate after activation at 375 °C (Fig. 7), and, at the same time, it reveals the presence of acidic P—OH groups. On the other hand, these acid sites are strong because about 33–40% of pyridine bonded to Brönsted acid sites is maintained after evacuation at 300 °C. In contrast, the concentration of Lewis sites is largely reduced after evacuation at high temperatures. The total concentration of acid sites ($C_B + C_L$) determined by pyridine adsorption is lower than that found by $NH_3$-TPD, which can be explained by considering that pyridine is a base weaker than ammonia, and it can only titrate strong acid sites.

### 3.2. Catalytic activity

The catalytic activity of this mesoporous tantalum phosphate has been tested in the transesterification of sunflower oil with methanol under heterogeneous conditions. The influence of different kinetic parameters such as temperature and reaction time, amount of catalyst as well as the presence of free fatty acids, water and co-solvent in the reaction medium, has been evaluated. The stirring rate (600 rpm) and methanol/oil molar ratio (12/1) were kept constant in all the experiments. This high methanol/oil molar ratio was used to favour the biodiesel formation [46].

Firstly, the catalytic behaviour of the mesoporous tantalum phosphate as a function of the reaction time has been studied by using the following experimental conditions: sunflower oil = 10 g, methanol/oil molar ratio = 12, amount of catalyst with respect to the oil weight= 5 wt.% and reaction temperature = 200 °C. From Fig. 8, it can be deduced that reaction rate is relatively high, since after 4 h of reaction 100 wt.% of oil conversion is attained with a biodiesel yield close to 93 wt.%, being detected mono and diglycerides as by-products. By taking into account that after 2 h of reaction good sunflower oil conversion is obtained (93 wt.%), with 88.9 wt.% of biodiesel yield, 2 h of reaction was selected to optimise the other parameters of the catalytic reaction.

As the next step, the influence of the reaction temperature was studied by using 0.50 g of catalyst at temperatures ranging between 175 and 200 °C, and 2 h of reaction time. This is a key parameter influencing the biodiesel production, since at 175 °C the biodiesel yield barely reaches 40 wt.%, being the oil conversion of 48 wt.% (Fig. 9). The maximum biodiesel yield is attained at 200 °C, with 88.9 wt.% and a conversion of the sunflower oil of 93 wt.%. For this reason, 200 °C was the temperature chosen for the study of the other experimental parameters. According to these results, this catalyst seems to be one of the most active and fast among those

**Table 1**
Textural parameters and acidity of mesoporous tantalum phosphate.

| Sample | BET surface area, $S$ ($m^2\,g^{-1}$) | Pore volume, $V_p$ ($mL\,g^{-1}$) | Average pore diameter, $d_p$ | Wall thickness (nm) | Total acidity ($\mu mol\,NH_3\,g^{-1}$) | Strong acidity (300–550 °C) ($\mu mol\,NH_3\,g^{-1}$) |
|---|---|---|---|---|---|---|
| $TaOPO_4$-550 | 255.7 | 0.18 | 2.8 | 4.9 | 1480 | 487 |
| $TaOPO_4$-750 | 146.0 | 0.20 | 5.5 | 2.6 | 989 | 169 |
| $TaOPO_4$-1000 | 8.3 | 0.02 | – | – | 371 | 286 |

**Table 2**
Concentration of Brönsted and Lewis acid sites ($\mu mol\,g^{-1}$), as determined by FTIR spectroscopy of adsorbed pyridine.

| Evacuation temperature (°C) | $TaOPO_4$ (evacuated at 25 °C) | | $TaOPO_4$ (evacuated at 250 °C) | | $TaOPO_4$ (evacuated at 375 °C) | |
|---|---|---|---|---|---|---|
| | $C_B$ | $C_L$ | $C_B$ | $C_L$ | $C_B$ | $C_L$ |
| r.t. | 288 | 36 | 309 | 97 | 290 | 50 |
| 100 | 281 | 32 | 265 | 50 | 229 | 14 |
| 200 | 196 | 29 | 184 | 35 | 184 | 3 |
| 300 | 113 | 20 | 101 | 17 | 126 | 0 |

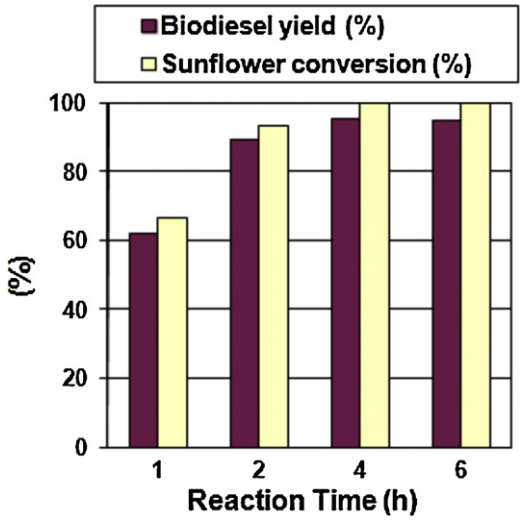


**Fig. 8.** Influence of the reaction time on the oil conversion and the biodiesel formation in the methanolysis of sunflower oil with mesoporous tantalum phosphate catalyst (reaction conditions: methanol/oil molar ratio = 12, catalyst = 5 wt.%, $T$ = 200 °C).

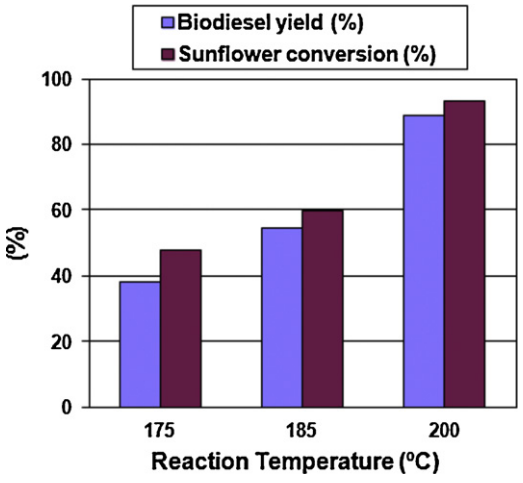


**Fig. 9.** Influence of the reaction temperature in the transesterification of sunflower oil with methanol (reaction conditions: methanol/oil molar ratio = 12, catalyst = 5 wt.% and reaction time = 2 h).

reported in literature for the preparation of biodiesel by heterogeneous acid catalysis [8]. The contribution of the un-catalysed thermal reaction has been measured under these experimental conditions (2 h of reaction at 200 °C), and the value found for the biodiesel formation was almost negligible [29]. It is noteworthy the high activity of this mesoporous tantalum phosphate, specially in a short time of reaction (2 h), which could be a consequence of its high acidity (Tables 1 and 2) and mesoporous structure that facilitate the easy access of the triglyceride molecules to the active sites. Furthermore, when the mesoporous tantalum phosphate is activated at 375 °C, and employed in the transesterification reaction, leads to the same FAME yield than the hydrated catalyst. This is a consequence of the high acidity still present after evacuation at 375 °C, with a total acidity of 340 μmol pyridine $g^{-1}$ (Table 2).

An essential aspect in the biodiesel production under heterogeneous conditions is the evaluation of the leaching of the active phase, $TaOPO_4$, in the reaction medium. With this purpose, the presence of both tantalum and phosphorus in the filtered solution, after the transesterification reaction during 2 h at 200 °C, has been analysed by ICP. The analytical results reveal that leaching is practically negligible due to the concentration of tantalum found in the reaction liquids is lower than 52 ppb, whereas the concentration of phosphorus was 138 ppb. These results were expected due to the low solubility of the mesoporous tantalum phosphate in organic media, and reveal its high stability under the experimental conditions used in the transesterification of sunflower oil with methanol.

Since the catalyst concentration affects the formation of FAME, the influence of the amount of catalyst in the transesterification reaction has been also evaluated, using loadings varying between 1 and 5 wt.% of catalyst with respect to the oil weight. The data (Fig. 10) reveal that the oil conversion and biodiesel formation increase monotonically with the amount of catalyst, achieving a maximum of 88.9 wt.% when the loading of catalyst was 5 wt.%. The evolution of the oil conversion and FAME yields are a lineal function of the catalyst weight, clearly indicating the absence of diffusional limitations of reactants or products in the catalytic reaction.

On the other hand, the presence of high concentrations of FFAs in low cost feedstocks, like cooking oils, may have adverse effects on the catalytic activity. A suitable solid acid catalyst has to be able to simultaneously carry out both esterification of FFAs and transesterification of oils. The influence of FFAs on the biodiesel formation was studied by adding different amounts of oleic acid to 10 g of sunflower oil in such a way that the resulting mixtures simulate used frying oils with acidity values ranged from 1° to 9° (defined as g of oleic acid per 100 g of oil). The data displayed in Fig. 11 reveal that the presence of FFAs does not influence on the transesterification

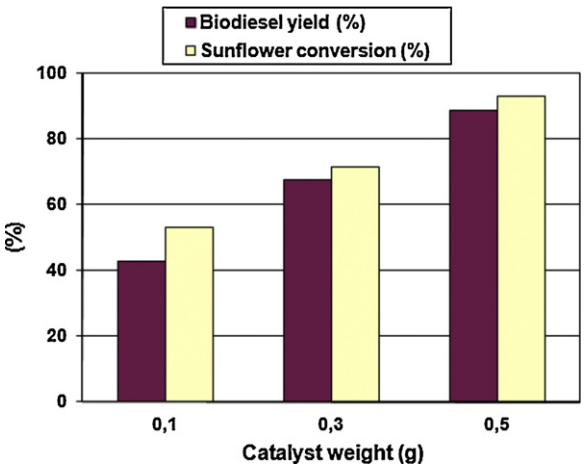


**Fig. 10.** Variation of the FAME yield in the methanolysis of sunflower oil as a function of the catalyst loading (reaction conditions: methanol/oil molar ratio = 12, $T$ = 200 °C and reaction time = 2 h).

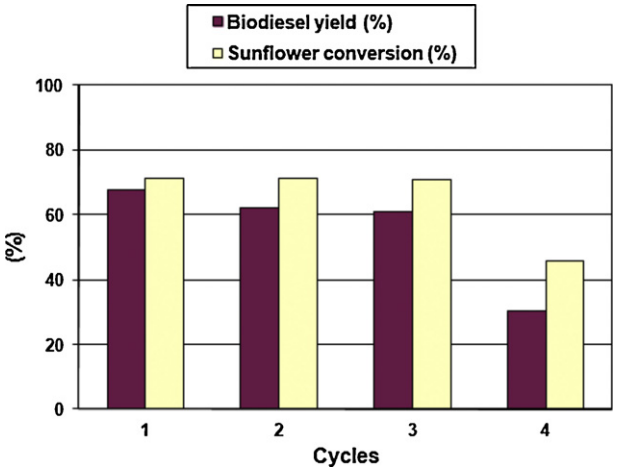


**Fig. 12.** Reusability test of the mesoporous tantalum phosphate catalyst in the methanolysis of sunflower oil (reaction conditions: methanol/oil molar ratio = 12, catalyst = 3 wt.%, $T$ = 200 °C and reaction time = 2 h).

activity; in contrast, the solid acid catalyst is able to produce the simultaneous esterification of FFAs and the transesterification of sunflower oil.

The results concerning the influence of the presence of water (5 wt.%) in the reaction medium demonstrate that the conversion and FAME yield were completely preserved (67 wt.% of FAME yield). This result was expected because the mesoporous tantalum phosphate was used in the catalytic reaction having a 4.7 wt.% of humidity, as deduced from the TG analysis. These water molecules could form water rich clusters around protons, which high acid strength enable to produce the transesterification reaction. This fact can explain the presence of strong acidity on this hydrous mesoporous tantalum phosphate, as is indicated in Table 1, with an amount of strong acid sites of 487 $\mu$mol $NH_3$ $g^{-1}$. Therefore, a moderate increment of the amount of water in the reaction medium seems not to affect to the acid strength, and thus the initial activity is fully preserved.

In order to evaluate the reusability of this mesoporous tantalum phosphate in the transesterification of sunflower oil, the catalyst was recovered from the reaction medium after each catalytic run by decantation and was reused for additional runs without any treatment as washing or calcination. The results confirm the stability of this catalyst, since the catalytic activity is well maintained with an average FAME yield of 63 wt.% during three cycles of reaction (Fig. 12). However, a loss of activity is observed during the fourth cycle. From these data, it could be deduced that on this catalyst take place, along of the successive reactions, strong surface adsorption of intermediates or reaction product more polar than the reactants [47] and/or carbon deposits [48–50]. In fact, after this fourth cycle of reaction, the content of carbon of the spent catalyst was 4.3 wt.%.

Finally, the influence of a co-solvent in the process of preparation of biodiesel, such as toluene, was also studied by incorporating 10 and 15% (v/v). of this solvent in the reactants (Fig. 13). By using 0.3 g of catalyst and after 2 h of reaction at 200 °C, the biodiesel formation were in both cases slightly lower than the value obtained without the use of co-solvent. Since toluene is a good solvent for vegetable oils and miscible with methanol, it was expected a little increase in the yield of biodiesel after the addition of this co-solvent. This decrease in both conversion and FAME yield indicates a dilution effect on the reactants and consequently a decrease in the rate of the process. Thus, after 2 h of reaction, the conversion and yield of FAME are lesser. In conclusion, in this reaction the use of toluene as co-solvent is not recommended.

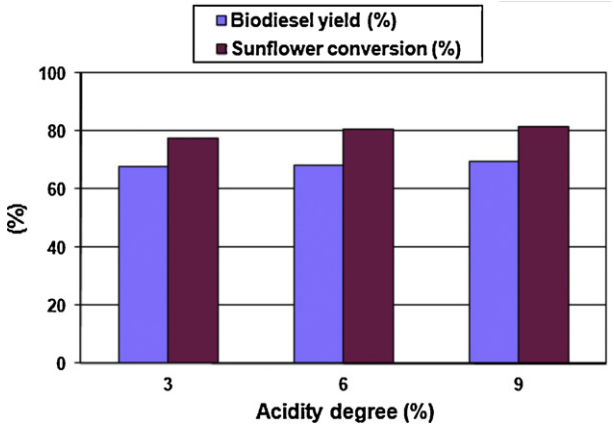


**Fig. 11.** Dependence of the biodiesel yield on the presence of free fatty acids in the methanolysis reaction (reaction conditions: methanol/oil molar ratio = 12, catalyst = 3 wt.%, $T$ = 200 °C and reaction time = 2 h).

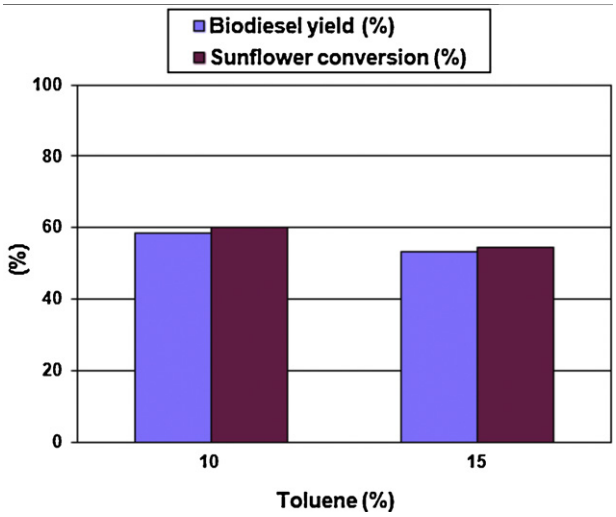


**Fig. 13.** Influence of toluene as co-solvent in the methanolysis of sunflower oil (reaction conditions: methanol/oil molar ratio = 12, catalyst = 3 wt.%, $T$ = 200 °C and reaction time = 2 h).

## 4. Conclusions

Mesoporous tantalum phosphate is a solid catalyst with a high specific surface area (256 $m^2\ g^{-1}$) and acidic character, with a total acidity of 1480 $\mu mol\ NH_3\ g^{-1}$, which enables to catalyse the transesterification reaction of sunflower oil with methanol. The best property of this new catalyst is its stability in this reaction at 200 °C, where no leaching of tantalum or phosphorus was detected. Moreover, this mesoporous tantalum phosphate is very active in this reaction since with only 5 wt.% of catalyst 89 wt.% of FAME is obtained after only 2 h of reaction; furthermore, it maintains a high percentage of its activity after three cycles of reaction. On the other hand, this catalyst is able to simultaneously produce the full esterification of FFAs and the transesterification of an oil with acidity up to 9°, at temperatures as low as 200 °C and in the presence of 5 wt.% of water.

## Acknowledgements

The authors are grateful to financial support from the Spanish Ministry of Science and Innovation (ENE2009-12743-C04-03 project) and Junta de Andalucía (P09-FQM-5070) and FEDER founds. IJM would like to thank the Agencia Estatal CSIC for a JAE-Predoctoral grant.

## References

[1] F. Ma, M.A. Hanna, Bioresource Technology 70 (1999) 1–15.
[2] K. Jacobson, R. Gopinath, L.C. Meher, A.K. Dalai, Applied Catalysis B: Environmental 85 (2008) 86–91.
[3] M.G. Kulkarni, A.K. Dalai, Industrial and Engineering Chemistry Research 45 (2006) 2901–2913.
[4] J.M. Marchetti, V.U. Miguel, A.F. Errazu, Fuel Processing Technology 99 (2009) 740–748.
[5] M. Hara, ChemSusChem 2 (2009) 129–135.
[6] E. Lotero, Y. Liu, D.E. Lopez, K. Suwannakarn, D.E. Bruce, J.G. Goodwin Jr., Industrial & Engineering Chemistry Research 44 (2005) 5353–5363.
[7] M. Di Serio, R. Tesser, L. Pengmei, E. Santacesaria, Energy & Fuels 22 (2008) 207–217.
[8] J.A. Melero, J. Iglesias, G. Morales, Green Chemistry 11 (2009) 1285–1308.
[9] I.K. Mbaraka, B.H. Shanks, Journal of American Oil Chemists' Society 83 (2006) 79–91.
[10] D.E. López, J.G. Goodwing Jr., D.A. Bruce, Journal of Catalysis 245 (2007) 381–391.
[11] S. Furuta, H. Matsuhashi, K. Arata, Biomass and Bioenergy 30 (2006) 870–873.
[12] Y.M. Park, D.W. Lee, D.K. Kim, J.S. Lee, K.Y Lee, Catalysis Today 131 (2008) 238–243.
[13] Y.M. Park, S.H. Chung, H.J. Eom, J.S. Lee, K.Y. Lee, Bioresource Technology 101 (2010) 6589–6593.
[14] C. Martins Garcia, S. Texeira, L. Ledo, Marciniuk, U. Schuchardt, Bioresource Technology 99 (2008) 6608–6613.
[15] B. Fu, L. Gao, L. Niu, R. Wei, G. Xiao, Energy & Fuels 23 (2009) 569–572.
[16] J.C. Juan, J. Zhang, Y. Jiang, W. Cao, M.A. Yarmo, Journal of Molecular Catalysis A: Chemical 272 (2007) 91–95.
[17] J.C. Juan, Y. Jiang, X. Meng, W. Cao, M.A. Yarmo, J. Zhang, Materials Research Bulletin 42 (2007) 1278–1285.
[18] K.N. Rao, D.R. Brown, A.F. Lee, A.D. Newman, P.F. Siril, S.J. Tavener, K. Wilson, Journal of Catalysis 248 (2007) 226–234.
[19] J.C. Juan, J. Zhang, M.A. Yarmo, Journal Molecular Catalysis A: Chemical 267 (2007) 265–271.
[20] K. Srilatha, N. Lingaiah, B.L.A. Prahbavathi Devi, R.B.N. Prasad, S. Venkateswar, P.S. Sai Prasad, Applied Catalysis A: General 365 (2009) 28–33.
[21] M. Di Serio, M. Cozzolino, R. Tesser, P. Patrono, F. Pinzari, N. Bonelli, E. Santacesaria, Applied Catalysis A: General 320 (2007) 1–7.
[22] K. Tanabe, Catalysis Today 8 (1990) 1–11.
[23] K. Tanabe, Catalysis Today 78 (2003) 65–77.
[24] K.P. Mendelssolm, L.C.P. Almeida, R. Landers, R.C.G. Vinhas, F.J. Luna, Reaction Kinetics, Mechanisms and Catalysis 99 (2010) 269–280.
[25] L. Xu, X. Yang, X. Yu, Y. Guo, Maynurkader, Catalysis Communications 9 (2008) 1607–1611.
[26] L. Xu, Y. Wang, X. Yang, X. Yu, Y. Guo, J.H. Clark, Green Chemistry 10 (2008) 746–755.
[27] L. Xu, W. Li, J. Hu, X. Yang, Y. Guo, Applied Catalysis B: Environmental 90 (2009) 585–594.
[28] L. Xu, W. Li, J. Hu, K. Li, X. Yang, F. Ma, X. Yu, Y. Guo, Journal of Materials Chemistry 19 (2009) 8571–8579.
[29] C. Sancho-García, R. Moreno-Tost, J. Mérida-Robles, J. Santamaría-González, A. Jiménez-López, P. Maireles-Torres, Applied Catalysis B: Environmental 108–109 (2011) 161–167.
[30] I. Jiménez-Morales, J. Santamaría-González, P. Maireles-Torres, A. Jiménez-López, Applied Catalysis A: General 405 (2001) 83–100.
[31] A. Sarkar, P. Pramanik, Journal of Non-Crystalline Solids 356 (2010) 2709–2713.
[32] A. Corma, Chemical Reviews 97 (1997) 2373–2420.
[33] J.M. Longo, J.W. Pierce, A. Kalafas, Materials Research Bulletin 6 (1971) 1157–1166.
[34] W. Weng, M. Davies, G. Whiting, B. Solsona, C.J. Kiely, A.F. Carley, S.H. Taylor, Physical Chemistry Chemical Physics 13 (2011) 17395–17404.
[35] M.L.C.P. da Silva, G.L.J.P. da Silva, D.N. Villela Filho, Materials Research 5 (1) (2002) 71–75.
[36] V.G. Ponomareva, V.A. Tarnopol, A.B. Yaroslavtsev, Russian Journal of Inorganic Chemistry 51 (3) (2006) 343–346.
[37] H.J. Ahn, K.W. Park, Y.E. Sung, Chemistry of Materials 16 (2004) 1991–1995.
[38] H.J. Ahn, H.S. Shim, Y.S. Kim, C.Y. Kim, T.Y. Seong, Electrochemistry Communications 7 (2005) 567–571.
[39] E. Parapazzo, E. Severini, A. Jiménez-López, P. Maireles-Torres, P. Olivera-Pastor, E. Rodríguez-Castellón, A.A.G. Tomlinson, Journal of Materials Chemistry 2 (11) (1992) 1175–1178.
[40] M. Baltes, A. Kytökivi, B.M. Weckhuysen, R.A. Schooheydt, P. Van Der Voort, E.F. Vansant, Journal of Physical Chemistry B 105 (2001) 6211–6220.
[41] J.C.G. da Silva, M.D. Viera, W. de Oliveira, Andrade, A.C.B. dos Santos, Journal of Materials Science 40 (2005) 4455–4460.
[42] J.Y. Zhang, I.W. Boyd, M.B. Mooney, P.K. Hurley, J.T. Beechinor, B.J. OïSullivan, P.V. Kelly, G.M. Crean, J.P. Senateur, C. Jimenez, M. Pailous, Applied Physics A 70 (2000) 647–649.
[43] K. Nakamoto, Infrared Spectra of Inorganic and Coordination Compounds, 2nd edition, Wiley-Interscience, New York, 1970, p. 110.
[44] Y.H. Pai, C.C. Chou, F.S. Shieu, Materials Chemistry and Physics 107 (2008) 524–527.
[45] J. Dakta, A.M. Turek, J.M. Jehng, I.E. Wachs, Journal of Catalysis 141 (1992) 186–199.
[46] D.Y.C. Leung, X. Wu, M.K.H. Leung, Applied Energy 87 (2010) 1083–1095.
[47] D.E. López, J.G. Goodwin Jr., D.A. Bruce, E. Lotero, Applied Catalysis A: General 295 (2005) 97–105.
[48] K. Suwannakarn, E. Lotero, J.G. Goodwin Jr., C. Lu, Journal of Catalysis 255 (2008) 279–286.
[49] G.X. Yu, X.L. Zhou, C.L. Li, L.F. Chen, J.A. Wang, Catalysis Today 148 (2009) 169–173.
[50] M.G. Kulkarni, R. Gopinath, L.C. Meher, A.K. Dalai, Green Chemistry 8 (2006) 1056–1062.